Supporting Information

Lipid Packing Drives the Segregation of Transmembrane Helices into Disordered Lipid Domains in Model Membranes

Lars V. Schäfer, Djurre H. de Jong, Andrea Holt, Andrzej J. Rzepiela, Alex H. de Vries, Bert Poolman, J. Antoinette Killian, and Siewert J. Marrink

Content:

1) Lateral diffusion of WALPs: Comparing experimental and simulation time scales

Simulation times from coarse-grained molecular dynamics (CG-MD) simulations can be compared to real times by accounting for the smoother energy landscape of CG models as compared to atomistic models: Since CG models lack (part of) the friction due to motion of the atoms, the dynamics observed in CG-MD simulations is faster than at the atomistic level. For the MARTINI CG model, a time conversion factor of 4 was found adequate to match the simulated and experimental diffusion coefficients of both bulk water and DPPC lipids in a bilayer. However, this time conversion factor cannot *a priori* be expected to be applicable to other processes as well, since it depends on the energy barriers and the relevant mass and length scales involved in the process under study. Here, to convert the simulation times from our CG-MD simulations of membrane-embedded WALP peptides to experimental time scales, we simulated a WALP23 peptide in dioleoylphosphatidylcholine (DOPC) bilayers, and compared the obtained lateral diffusion coefficient to experiments (1, 2).

MD simulations. Two CG-MD simulations using the MARTINI model were carried out, in which a single WALP23 peptide was embedded into a pre-equilibrated bilayer of 476 DOPC molecules solvated by 6816 CG water beads (one CG water bead represents 4 water molecules). In the first simulation, a 14-bead MARTINI model was used for DOPC, in which each lipid chain comprised 5 beads. In the second simulation, DOPC comprised 12 beads, i.e., only 4 beads per chain. In both cases, the lipid chains contained a C3-type bead (in the third position), which together with the appropriate bonded parameters models the double bond. These two different models were used, because the

measured thicknesses of DOPC bilayers can vary substantially (depending on the experimental conditions), with a typical range between 3.7 and 4.3 nm. The 12- and 14-bead DOPC models yield a bilayer thickness of about 3.90 and 4.35 nm, respectively, a range comparable to that observed in experiments. The systems were equilibrated for 200 ns prior to data collection. NpT ensembles were simulated at 300 K, with the simulation parameters as described in Methods. The simulation time was 4 μs for each system.

Lateral diffusion. The lateral diffusion coefficient of the peptide was calculated from the long time mean square displacement (msd) of the peptide over time according to

$$D_{lat} = \lim_{t\to\infty} \frac{\left\langle \left| r(t+t_0) - r(t_0) \right|^2 \right\rangle}{4t},$$

where r is the center of mass vector of the peptide in the membrane plane. The time window averaging was done over all initial time origins t_0. The overall center of mass motion was removed. The statistical error was obtained by separately analyzing the two halves of the trajectory. The obtained msd curves, shown in Figure S1, are to a good approximation linear over the time interval 10 to 100 ns. Linear fits yield D_{lat} = 15.6 ± 2.4 $\mu m^2/s$ and 23.2 ± 2.0 $\mu m^2/s$ for WALP23 in the 14-bead and 12-bead DOPC bilayers, respectively, which are about 3 to 4.4 times larger as compared to the value of D_{lat} = 5.3 $\mu m^2/s$ measured in giant unilamellar vesicles composed of pure DOPC (1) or of a 3:1 mixture of DOPC and DOPG (2). Thus, we conclude that a factor of about 4 is appropriate to convert the peptide diffusion time observed in our CG-MD simulations to the experimental time scale. Unless stated otherwise, all times reported in the main text are effective times, that is, simulation times multiplied by a factor 4.

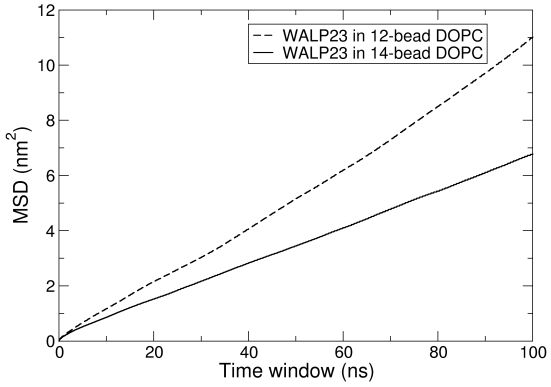

Figure S1. Mean square displacement of a single WALP23 in a 12-bead (dashed line) and a 14-bead (solid line) DOPC bilayer. The lateral diffusion coefficient was obtained from a linear fit to the msd curve in the time interval 10 to 100 ns (simulation time).

2) TI calculations of partitioning free energy

Here we describe the details of the free energy calculations presented in the main manuscript. The full results of the thermodynamic integration (TI) simulations are summarized in Table S1.

System setup. For the TI simulations, we used two bilayer patches with lipid compositions corresponding to the Lo and Ld domains, respectively. The Lo bilayer patch comprised 368 di-C16:0PC and 224 cholesterol molecules, corresponding to a 0.62 : 0.38 molar ratio. The Ld bilayer patch comprised 336 di-C18:2PC, 32 di-C16:0PC, and 72 cholesterol molecules, corresponding to a 0.76 : 0.08 : 0.16 molar ratio. These mixtures closely match the equilibrium compositions in the core of the Lo and Ld domains, respectively (3). Initially, the PC and cholesterol molecules were randomly distributed in the membrane plane (with equal amounts of each molecule type in both monolayers), and the bilayers were solvated by 5328 CG water beads (one CG water bead represents 4 atomistic water molecules). Then, into both bilayers, a single WALP peptide was inserted in its transmembrane orientation. To generate starting structures for the subsequent simulations, the systems were energy minimized (steepest descent, 1000 steps) and equilibrated for 4 μs in free MD simulations, using the MARTINI force field and simulation parameters as described in Methods.

TI procedure. As shown in Figure S2, the free energies of extracting a peptide from the membrane bilayer to the gas phase were determined by thermodynamic integration with a coupling parameter λ. This was done in two steps: First, all non-bonded interactions of the peptide with the surrounding bilayer and water as well as within the peptide were turned off; second, the interactions were turned back on in vacuo. Thus, $\lambda = 0$ and $\lambda = 1$ correspond to the fully coupled and uncoupled states, respectively. Note, the helicity of the WALP peptides is imposed by the dihedral (bonded) interactions, and is thus not affected during the TI. From the free energies of extracting a peptide from the bilayer to the gas phase, the transfer free energy between the Lo and Ld domains was calculated as $\Delta G_{Lo/Ld} = \Delta G_{Lo/vac} - \Delta G_{Ld/vac}$. In the TI simulations, NpT ensembles were simulated using stochastic temperature coupling to T = 300 K and an inverse friction coefficient of 5 ps. This friction coefficient yields a similar lipid lateral diffusion coefficients as observed in the MD simulations of the large 2000-lipid bilayer. The center of mass of the peptide was kept close to the center of the bilayer by means of a harmonic position restraint along the bilayer normal (force constant 1000 kJ mol^{-1} nm^{-2}). This restraint prevents the peptide from slipping out of the bilayer at λ close to 1, while still allowing it to diffuse, reorient, and tilt in the bilayer. A soft-core potential was used for the nonbonded Lennard-Jones interactions (the WALP peptides bear no (partial) charges in the MARTINI force field), with potential-height $\alpha = 1.3$, λ-power = 1, and interaction-range $\sigma = 0.47$ nm (4). We used a basic spacing between the λ-points of 0.05; additional λ-points were added at $\lambda = 0.375$, $\lambda = 0.425$, and $\lambda = 0.475$, where the curvature of $dG/d\lambda$ is maximal (see Figure S2a), yielding a total of 24 λ-points. At each λ-point, the system was simulated for 500 ns (which, using the time conversion factor of 4 observed for DOPC bilayers, see above, may correspond to about 2 μs of atomistic simulation time). The first 20% of each simulation were considered equilibration and excluded from the analysis. Error estimates were obtained by fitting a bi-exponential function to the block average of $dG/d\lambda$ as a function of block size, as implemented in the g_analyze tool of Gromacs and described in Ref. (5).

Enthalpy estimation. To obtain the enthalpies, we carried out long MD simulations of the Lo and Ld bilayer patches with and without the peptides, and of the individual peptides in vacuo. The systems were simulated for 40 μs and 16 μs for the Lo and Ld bilayer patches, respectively, in addition to an initial equilibration phase of 4 μs. The vacuum systems were simulated for 100 ns. The enthalpies were calculated by subtracting the potential energy of the pure bilayer and the peptide in vacuo from the potential energy of the membrane-embedded peptide. We neglected the contribution $p\Delta V$, as it as small for condensed liquid phase systems at ambient pressures (here, $p\Delta V \approx 0.3$ kJ/mol for WALP31). We also neglected the contribution due to the liberation of the solute (6), as it is (i) smaller than the statistical error, and (ii) cancels out in the calculation of $\Delta H_{Lo/Ld}$. Error estimates (shown in Figure S2b) were determined by block averaging, see above.

Table S1. Free energies, enthalpies, and entropies obtained from TI simulations.[a]

	$\Delta G_{Lo/Ld}$	$\Delta G_{Lo/vac}$	$\Delta G_{Ld/vac}$	$\Delta H_{Lo/Ld}$	$\Delta H_{Lo/vac}$	$\Delta H_{Ld/vac}$	$-T\Delta S_{Lo/Ld}$	$-T\Delta S_{Lo/vac}$	$-T\Delta S_{Ld/vac}$
WALP23	-63 ± 8	678 ± 5	741 ± 5	-594 ± 47	71 ± 45	665±14	531 ± 48	607 ± 46	76 ± 15
WALP31	-58 ± 8	855 ± 5	913 ± 6	-276 ± 33	500± 32	776±10	218 ± 34	354 ± 32	137 ±12

[a] All values in kJ mol^{-1}. Results are obtained at T=300 K. $\Delta G_{Lo/vac}$ and $\Delta G_{Ld/vac}$ are the free energies of transferring a single peptide from the Lo and Ld bilayer patches, respectively, to the vacuum. $\Delta G_{Lo/Ld}$ was obtained as $\Delta G_{Lo/vac} - \Delta G_{Ld/vac}$. Standard errors are given. The statistical errors in Lo/Ld were obtained by assuming that the values in Lo/vac and Ld/vac are independent.

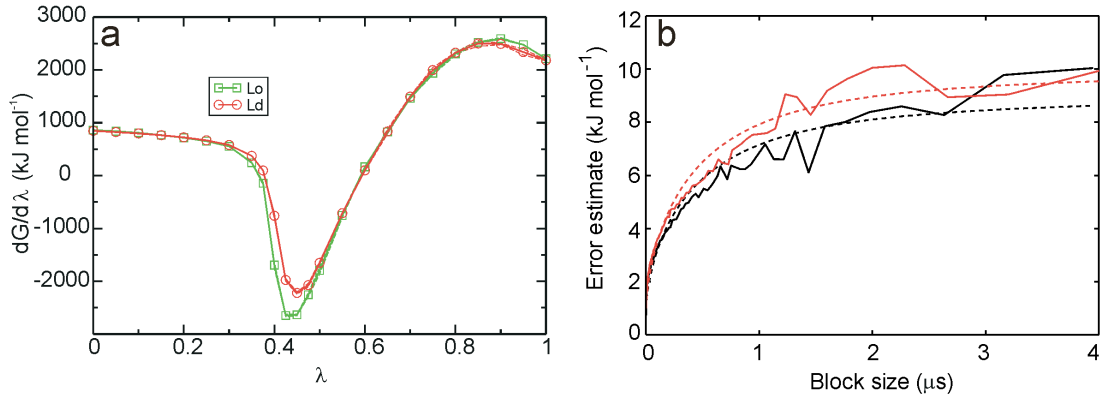

Figure S2. a) Results from thermodynamic integration simulations for WALP23. The green and red curves show the TI in the Lo and Ld bilayers, respectively. Statistical errors are plotted as dashed side-lines. Similar curves were obtained for WALP31. b) Convergence of the errors of the potential energy (used to estimate the enthalpy, see text) as a function of block size (solid lines), together with the analytical estimate (bi-exponential function, dashed lines) for the Ld bilayer without (black) and with WALP23 embedded (red).

Enthalpy – entropy compensation. As stressed in Table 1, the absolute numbers of the enthalpy and the entropy obtained with a coarse-grained model should be interpreted with care. However, the Lo/Ld partitioning *free energy* differences should be accurate. This may in particular be expected for the MARTINI model, because it was parameterized against experimental partitioning free energies. In

general, coarse-grained models have a smaller entropy than atomistic models due to the reduced number of degrees of freedom. Thus, to arrive at the desired correct free energy, this smaller entropy has to be compensated for by a corresponding change in enthalpy For more details on this topic, we refer to the work of Baron et al. (7, 8).

For the dimerization of WALP23 in DOPC, a direct comparison of enthalpies and entropies obtained from experiment and simulation is possible: Yano and Matsuzaki (9) measured values of $\Delta H = -31$ kJ/mol and $T\Delta S = +19$ kJ/mol, which can be compared to the respective values of –30 kJ/mol and +15 kJ/mol obtained by Ash and coworkers using the MARTINI force field (10). Thus, not only is the dimerization free energy difference ΔG obtained with the MARTINI model in good agreement with experiment, but also the enthalpic and entropic parts.

Our main conclusion here is that the peptide sorting is enthalpy-driven. This conclusion is of qualitative nature, independent of the exact values. It is based on the observation that the inclusion of a TM helix introduces substantial disorder (increases entropy) in the Lo domain, but not in Ld (see Table S1). Thus, solely in terms of entropy, the peptides would segregate into Lo, which is not observed. Our free energy calculations show that in Lo, the entropy gain is outplayed by an enthalpy loss, which is thus the driving force for the overall process. Also at the atomistic level, the degree of disorder introduced by inserting a TM peptide into the Lo domain can be expected to be larger than in the Ld domain, and again the entropic driving force towards Lo will have to be over-compensated by enthalpy. Of course, this only holds if the resulting free energy upon moving a peptide from Lo to Ld is negative not only at the CG but also at the atomistic level. This can be safely assumed to be the case, because it is also observed in the experiments.

To test our hypothesis, we calculated lipid chain order parameters using both CG and atomistic MD simulations. The results, given in the following section, support the idea that the peptide sorting is enthalpy-driven.

3) Lipid chain order parameters

We calculated lipid chain order parameters to substantiate the interpretation of our TI calculations, and further investigate the configurations of the lipids around the peptides, both using CG and atomistic simulations. Peptide-bound lipids are compared to bulk lipids.

Method. The second-rank order parameter,

$$P_2 = \frac{1}{2}\left(3\left\langle \cos^2\theta \right\rangle - 1\right),$$

was computed for consecutive bonds in the CG lipids, with θ the angle between the bond vector and the bilayer normal. The square brackets denote an ensemble average. Perfect alignment with the bilayer normal is indicated by $P_2 = 1$, perfect anti-alignment by $P_2 = -0.5$, and a random orientation by $P_2 = 0$. Order parameters were calculated by averaging over 100 evenly spaced snapshots taken from the last μs of the free simulations of the bilayer systems used in the TI simulations (see above). Figure S3 compares the order parameters of the lipids that are bound to the peptide to those of unbound lipids. A

lipid was considered bound to the peptide if the distance between its phosphate head group bead and any bead of the peptide was smaller than 0.8 nm. On average, 6 lipids were bound to a peptide. For the unbound lipids, the order parameters were averaged over all 368 and 336 di-C16:0PC and di-C18:2PC lipids present in the Lo and Ld peptide-free bilayers, respectively. In Ld, di-C18:2PC preferentially binds to the peptides, and thus the di-C16:0PC molecules in Ld were excluded from the analysis.

To obtain order parameters from atomistic simulations, two snapshots of WALP23 in the Lo and Ld bilayers, respectively (taken after 1000 ns of CG simulation) were back-mapped to their underlying atomistic representations using the reverse transformation procedure detailed in section 6 below. For both systems, a 60-ns atomistic MD simulation was carried out; the first 30 ns of each simulation were discarded as equilibration time (for simulation details, see section 6). Prior to analysis, the atomistic trajectories were converted to the MARTINI CG representation to enable a comparison to the order parameters directly obtained from the CG simulations (Figure S3).

Results. Figure S3 shows that in the Lo domain, peptide-bound lipids have a lower order parameter as compared to lipids in the bulk. This effect is more pronounced for CG di-C16:0PC lipids in the vicinity of WALP23 (Figure S3a, black line) than for those close to WALP31 (Figure S3a, blue line): The average chain order parameter (averaged over bonds 4-7) drops from 0.793 for CG di-C16:0PC in the bulk Lo phase to 0.645 for CG lipids bound to WALP23, a decrease of 19%. CG lipids bound to WALP31 have an average chain order parameter of 0.728, which is only 8% lower than in the bulk. In addition, lipids bound to WALP23 show a decreased P_2 for bond 2 in the PC head group, which is not the case for lipids bound to WALP31. Although P_2 order parameters cannot be straightforwardly translated into entropies, the observed decrease of P_2, which is about two times stronger for WALP23 than for WALP31, agrees very well with the entropy differences obtained from the TI calculations, see Table S1. In contrast to the ordered domain, inclusion of WALP23 or WALP31 into the Ld domain does not substantially influence the order parameters as compared to the peptide-free case (Figure S3b). Thus, the high degree of disorder already intrinsic to Ld is not further decreased by the peptide, in line with the small entropy gain upon peptide inclusion (Table S1).

The order parameters obtained from the atomistic simulations are shown in Figure S3c,d. In the Lo domain, bonds in peptide-bound di-C16:0PC chains have lower order parameters than in bulk lipids: The average chain order parameters (averaged over bonds 4-7) are 0.704 and 0.814 for peptide-bound and bulk lipids, respectively, a difference of 0.11. For di-C18:2PC lipids in the Ld domain, the respective values are 0.200 and 0.240, a difference of only 0.04. Thus, in agreement with the CG simulations, also in the atomistic simulations WALP23 does introduce substantial disorder in the Lo, but not in the Ld domain. Hence, also the atomistic simulations show that there is an entropic driving force for peptide sorting into Lo that has to be overcompensated by an enthalpic preference for Ld.

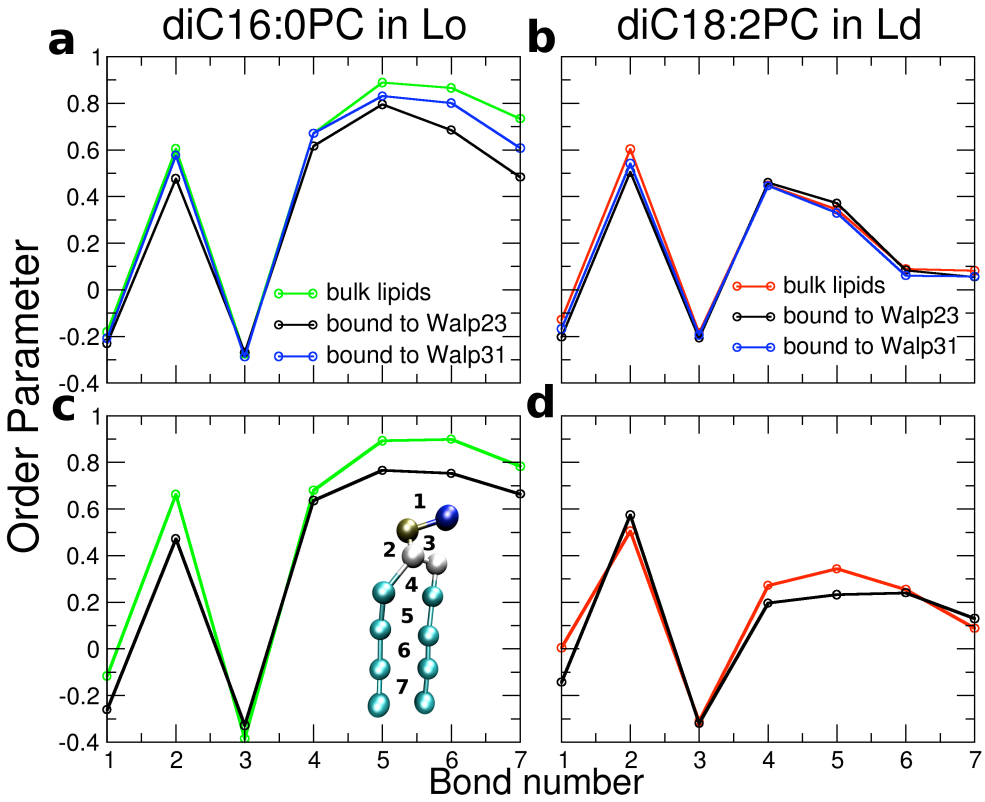

Figure S3. P_2 order parameters for consecutive bonds in PC lipids with respect to the bilayer normal. The data for bonds 4-7 are averaged over both lipid chains. The bond numbers are shown in c, inset. P_2 of CG di-C16:0PC in Lo (a) and CG di-C18:2PC in Ld (b) bound to WALP23 or WALP31 (black and blue lines, respectively), are compared to P_2 of bulk lipids in (peptide-free) Lo and Ld bilayers (green and red lines, respectively). Panels (c) and (d) show the respective order parameters obtained from atomistic simulations.

4) Crossing and tilt angles of WALP23 dimers and trimers

Here we present details about the clusters formed by the WALP23 peptide.

Crossing angles. Figure S4 shows that the crossing angle distributions for the right-handed dimers are rather broad, with a mean value at θ = -26.7° and a standard deviation of 6.6° (solid line). For trimers, θ = -24.4° and a standard deviation of 6.5° was found (dashed line). These crossing angles are slightly smaller than the -40° observed in the right-handed glycophorin A dimer (11). The inset of Figure S4b shows a representative crossing angle time trace for a WALP23 dimer (stable between 8 and 24 μs). The crossing angle displays transitions to values around -55° and -5° on the μs time scale, emphasizing the large conformational flexibility. To observe these rare events requires long time scales, as enabled by the use of CG models.

Tilt angles: The tilt angles (Figure S4) of single peptides were obtained from the extended simulations of the small bilayer patches used in the TI calculations and are summarized in Table S2. As expected,

the WALP23 peptide in Lo (negative mismatch) adopts the smallest tilt angle (8.8°). This tilt is very small, as it falls almost within the tilt due to thermal fluctuations. Under hydrophobic matching conditions, intermediate tilt angles of about 15° to 20° are observed, in very good agreement with data from experiments and other simulations (12, 13). WALP31 in Ld reacts on the extreme mismatch conditions by adopting a very large tilt angle of about 45°.

Table S2: Tilt angles of monomeric WALP peptides in Lo and Ld.

Peptide	Tilt angle in Lo (± std. dev.)*	Tilt angle in Ld (± std. dev.)*
WALP23	8.8° ± 4.7°	20.9° ± 9.3°
WALP31	13.7° ± 5.3°	45.3° ± 7.8°

*Statistical errors (obtained from block averaging, see above) are below 1°.

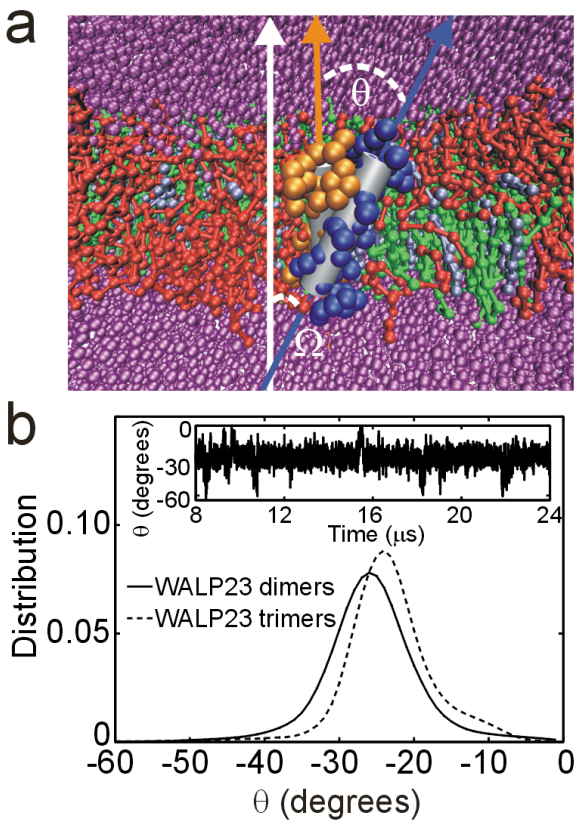

Figure S4. Crossing-angles of WALP23 dimers and trimers. a) Snapshot from CG-MD simulation showing a right-handed dimer of WALP23 molecules (side view). The two peptides are shown as orange and blue spheres, respectively; grey cylinders represent α-helices with an arrow along the helix axis. The white arrow shows the membrane normal. The inter-helix crossing-angle θ and helix tilt-angle Ω are indicated by dashed lines. di-C16:0PC and di-C18:2PC lipids are shown in green and red, respectively; cholesterol is colored grey; water is shown in purple. b) Distributions of crossing angles for WALP23 dimers (solid line) and trimers (dashed line). Inset: Representative crossing angle time-trace for individual WALP23 dimer.

Parallel vs. anti-parallel WALP23 dimers. In FRET experiments of Sparr and coworkers, a clear preference for an antiparallel arrangement of the WALP helices in a dimer was observed (14). In our simulations, we found a 4:1 ratio of antiparallel (AP) and parallel (P) WALP23 dimers, in qualitative agreement with the experiments. It was speculated that AP is preferred over P due to the favorable interaction between antiparallel helix-macrodipoles. Although the MARTINI model does not have explicit dipolar interactions between the helix backbones, the model differentiates between backbone beads close to the C- and N-termini of the helix in such a way that cross-interactions between C- and N-terminal backbone beads are more favorable than those between the same termini.

5) Partitioning of WALP31 with restricted tilt

Here we show that a WALP31 peptide that is restrained to an upright orientation prefers to reside at the domain boundary.

System setup. To study the partitioning of WALP31 in the absence of tilting, a single WALP31 transmembrane peptide was energy-minimized in vacuo (100 steps, steepest descent), and subsequently incorporated into the core of the Lo domain, such that it was not tilted with respect to the membrane normal. After 1000 steps of steepest descent energy minimization, a 20-μs MD simulation (MARTINI force field) was carried out, during which the motion of the backbone beads of residues 2 and 30 along the membrane normal (z-axis) was restricted through harmonic potentials (force constant 1000 kJ mol^{-1} nm^{-2}). This procedure yielded a reduced tilting of the peptide (mean tilt angle of about 10°).

Results. Figure S5 shows a series of snapshots from the simulation. Within the first 4 μs the WALP31 peptide diffuses to the domain boundary, where it stays for the rest of the simulation time.

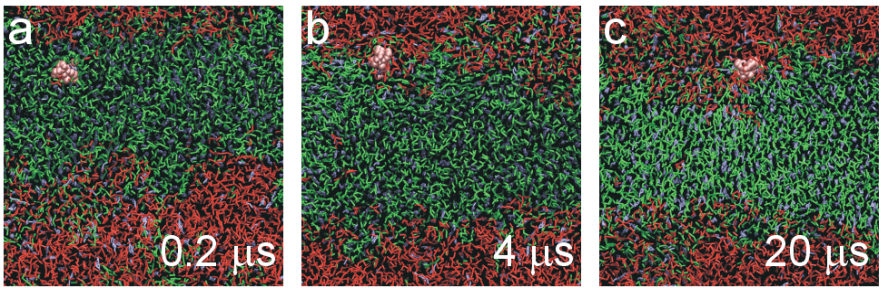

Figure S5. A WALP31 peptide that is not allowed to significantly tilt is located at the domain boundary. Snapshots after 0.2 (a), 4 (b), and 20 μs (c) of MD simulation; the color code is the same as in Figure 1.

6) Atomistic simulation

To test whether the peptides' clustering behavior might have been affected by the coarse-grained representation of the molecules, we also performed an MD simulation using an atomistic force field.

Methods. In the atomistic simulation, the peptides were described with the 53A6 parameter set of the Gromos force field (15), with the latest update on peptide backbone dihedral angle parameters that enhance the stability of α-helices (16). For the phosphatidylcholine lipids we used an in-house version of a new Gromos53A6-based lipid force field; parameters and additional information are obtainable from the authors upon request. Parameters for cholesterol were taken from Marrink et al. (17) and the SPC water model (18) was used. To obtain the starting structure for the atomistic simulations, a snapshot from the CG simulation of the WALP23 system was transformed to the underlying atomistic representation using our recent resolution transformation algorithm (19). During the resolution transformation, the system was cooled down from an initial temperature of 1300 K to the desired target temperature of 295 K by 100 ps of simulated annealing, during which the atomistic particles were coupled to their corresponding CG beads through harmonic restraints. Subsequently, the coupling was gradually removed within a time span of 10 ps. These annealing simulations were carried out in the NVT ensemble. No constraints were applied, and an integration time step of 1 fs was used. To control the temperature, stochastic coupling with an inverse friction constant $\tau_T = 0.1$ ps was applied. The other parameters for the resolution transformation were set to the standard values (19). During the subsequent free atomistic MD simulations, application of the Lincs (20, 21) and SETTLE (22) algorithms allowed for an integration time step of 2 fs. Temperature and pressure coupling was applied similar to the CG simulations, with time constants $\tau_T = 0.1$ ps and $\tau_p = 1$ ps, respectively. Non-bonded interactions within 0.9 nm were updated at every time step, and interactions between 0.9 and 1.4 nm every 10 steps. A reaction field contribution (23) was added to the electrostatic interactions beyond this long-range cutoff, with $\varepsilon_{rf} = 54$.

System details. The snapshot after t = 40 μs from the CG-MD simulation of the WALP23 system was transformed to the atomistic representation, followed by a free 100-ns atomistic MD simulation. Including peptides, lipids, and water molecules, the system comprised of about 241,000 particles. As summarized in Table S3, at the beginning of the atomistic simulation, there were four WALP23 dimers, one trimer, and one monomer. Two of the dimers contain antiparallel helices, whereas the other two dimers consist of parallel peptides (averaged over the CG simulation, the AP/P dimer ratio is 4:1, see above). There is one left-handed dimer (dimer4), whereas the other three dimers adopt the right-handed configuration. The peptides in the trimer form the typical linear arrangement: The central helix forms an antiparallel left-handed pair with one of the outer helices, and a parallel right-handed pair with the other.

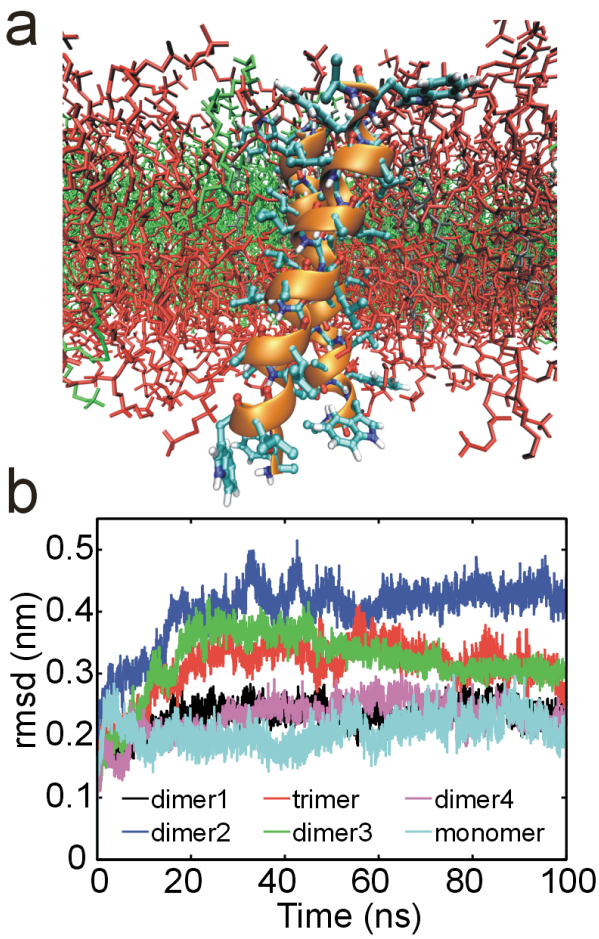

Figure S6. Atomistic molecular dynamics simulation of WALP23 system. a) Snapshot (side view) showing a zoom-in on an antiparallel right-handed WALP23 dimer (dimer3, Table S3) after 100 ns of simulation. The peptides are shown in ball-and-sticks representation with α-helices colored orange. Lipid molecules are shown as thin sticks, water molecules are not shown for clarity. The color code is the same as in Figure 1. b) Root-mean-square deviation (rmsd) of peptide C_α-atoms with respect to starting configuration.

Table S3: Peptide clusters in WALP23 system after t = 40 μs of CG-MD simulation.

Cluster	P / AP	Handedness	C_α-rmsd after 100 ns atomistic MD
dimer1	AP	RH	0.24 nm
dimer2	P	RH	0.41 nm
dimer3	AP	RH	0.29 nm
dimer4	P	LH	0.29 nm
trimer	AP, P	LH, RH	0.23 nm
monomer	-	-	0.22 nm

P = parallel; AP = antiparallel; RH = right-handed; LH = left-handed

Results. Figure S6a shows a zoom-in on the antiparallel right-handed dimer3 (Table S3) after 100 ns of atomistic simulation; the C_α-rmsd time traces of the peptides during the atomistic simulation are shown in Figure S6b. The final rmsd of the oligomers with respect to their starting configuration (the back-mapped CG configuration) is summarized in Table S3. All peptides stay α-helical during the simulation. Three of the dimers (dimer1, dimer3, and dimer4) as well as the trimer stay bound, as indicated by an rmsd < 0.3 nm. Such low rmsd values are typical for atomistic MD simulations of small proteins (i.e., of comparable size to the WALP peptides) in the absence of large-scale conformational changes. The parallel dimer2, however, dissociates, and the two peptides become separated by lipid molecules. This single dissociation event shows that the simulation time of 100 ns, although considered short, can in principle be sufficient to probe the stability of the oligomers. This conclusion is also supported by the rmsd curves in Figure S6b, which do not show a steady rise over the simulation time. Although the atomistic simulations are computationally too demanding to be able to yield a fully equilibrated ensemble, the results are consistent with the conclusions drawn from our CG simulations: WALP23 peptides in the Ld phase form stable dimers and trimers, with occasional dissociation (and, on longer time scales, re-association) events.

7) Coarse-grained MD simulation of TM domain of syntaxin 1A

We carried out an additional CG-MD simulation of the α-helical transmembrane region of the syntaxin 1A (Sx1A) protein. Sx1A partitions into the Ld domain and forms weakly bound clusters.

System Setup. An atomistic α-helical structure of the TM domain of murine syntaxin 1A (TM-Sx1A, residues 259-288, sequence SKARRKKIMIIICCVILGIIIASTIGGIFG) was constructed using the pepbuild webserver (www.imtech.res.in/bvs/pepbuild) and converted into its CG representation. The subsequent MD simulation protocol used was very similar to the one applied for the WALP peptides: Initially, nine TM-Sx1A proteins were inserted into the same phase-separated lipid bilayer that was used for the WALP simulations; the TM-Sx1A helices were regularly distributed on a lateral grid. All nine proteins were inserted in a parallel manner, such that the basic aminoacids at the N-terminus are located at the same side of the membrane. After energy minimization and a short MD with positional restraints on the protein beads, the system was simulated for 8 μs (simulation time) using the MARTINI force field (simulation parameters identical to those applied in the WALP simulations). The C-terminus was capped with a negative charge, whereas the N-terminus was capped with an uncharged P4-type bead. The helicity of TM-Sx1A (24) was kept stable by dihedral potentials, similar to the WALPs.

Results. The observed partitioning and clustering of TM-Sx1A closely resembles that of WALP23 in that TM-Sx1A segregates into the Ld domain and forms small clusters, with frequent association / dissociation events on the μs time scale. Figure S7 shows a typical configuration, taken after 5 μs of simulation time. All proteins are located in the Ld domain, where they form (mostly) dimers and trimers that are in equilibrium with monomeric proteins.

Figure S7. Snapshot after 5 μs of simulation time. Syntaxin 1A proteins are shown as colored spheres. Color code the same as in Figure 1.

8) Coarse-grained MD simulations of TM domain of the linker for activation of T cells (LAT)

Additional CG-MD simulations of the transmembrane domain of the linker for activation of T cells (LAT) protein (25) were carried out, using both palmitoylated and non-palmitoylated forms.

System Setup. An atomistic α-helical structure of the TM domain of LAT (EADWLSPVGLGLLLLPFLVTLLAALCVRCRE, residues 2–32 of murine LAT, with substitution Trp for Ala^{4}) was constructed using the pepbuild webserver (www.imtech.res.in/bvs/pepbuild) and converted into its CG representation. Two MD simulations were carried out. In the first simulation, palmitoyl anchors were attached to both terminal Cys residues (26), whereas in the second simulation, non-palmitoylated LAT was used. The simulation protocol was identical to the one applied for TM-Sx1A (see above): Initially, nine LAT proteins (regularly distributed on a lateral grid) were inserted into the bilayer, in a parallel manner. After energy minimization and a short MD with positional restraints on the protein beads, both the palmitoylated and non-palmitoylated LAT systems were simulated for 11 μs (simulation time), using the MARTINI force field (same simulation parameters as used above). Both termini were capped with uncharged P4-type beads; the helicity of residues 3 – 28 was kept stable through dihedral potentials.

Results. In agreement with experiments on model membranes (27), LAT TM domains partition into the Ld domain, irrespective of bound palmitoyl anchors. Due to the initial placement of monomeric proteins in the membrane, the LATs first sequester as monomers into Ld, where they form clusters. The clustering behavior is different for palmitoylated and non-palmitoylated LAT: For the former, occasional dissociations of clusters are observed, whereas non-palmitoylated LAT clusters do not break up again within the simulation time. The stronger clustering of LAT is similar to WALP31, due to the comparably long hydrophobic stretches. The monomeric LATs sample both the Lo/Ld interface and the

bulk Ld domain. The LAT clusters also prefer Ld, but remain close to the interface (see Figure S8) and do not return to the core of the Ld domain on the time scale of our simulations.

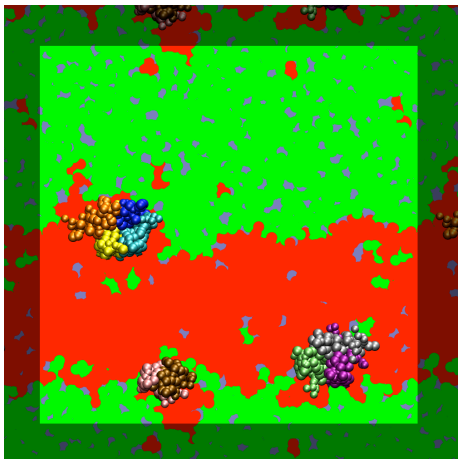

Figure S8. Representative snapshot (after 11 μs of simulation time) from CG-MD simulation of palmitoylated LAT TM domains. Here, the LATs (shown as colored spheres) form a dimer (lower left), a trimer (lower right), and a tetramer (middle left). Color code the same as in Figure 1.

9) Coarse-grained MD simulations of palmitoylated WALP23 peptides

Two additional CG-MD simulations were carried out. In the first simulation, two palmitoyl anchors were attached to WALP23, whereas in the second simulation, eight palmitoyl anchors per peptide were used. The doubly palmitoylated peptides partition into the Ld domain, as was also observed in experiments (28), whereas the octa-palmitoylated WALP23 peptides are located at the domain boundary interface.

System Setup. The system setup and simulation parameters were the same as for the non-palmitoylated WALPs described above. For the doubly palmitoylated WALP, both palmitoyl anchors were attached to the side chain of an additional Glu residue attached to the N-terminus of the peptide. To generate the octa-palmitoylated peptides, four palmitoyl tails were attached to the N- and C-terminal residues, respectively. The simulation times were 9 μs, respectively.

Results. The partitioning and clustering of the doubly-palmitoylated WALP23 peptides does not substantially differ from that of their non-palmitoylated counterparts. Peptides carrying eight palmitoyl anchors also preferentially partition into the Ld domain, however, they are bound to the domain boundary interface (see Figure S9). The fluctuations of the interface are enhanced, suggesting a reduced line tension. Such poly-palmitoylated peptides are thus potential line-active molecules, a prediction that can be tested experimentally.

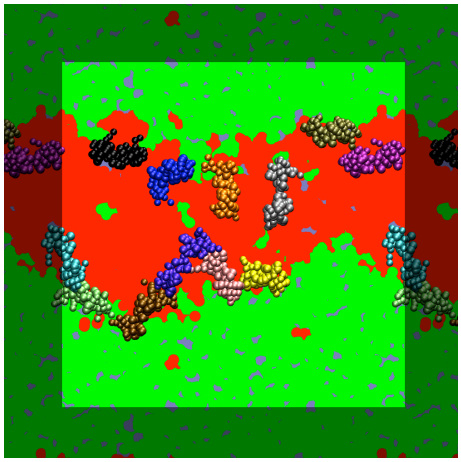

Figure S9. Snapshot (after 9 μs of simulation time) from CG-MD simulation of octa-palmitoylated WALP23 shows the partitioning at the domain boundary interface. Color code the same as in Figure 1.

10) Dimerization free energy of WALP23: Statistical error, comparison to literature

As described in the main text, we estimated the association constant *K* of WALP23 in the Ld domain form the average number of monomers and dimers observed during the simulation. For this analysis, the first 20 μs of the 80 μs simulation were discarded as equilibration time. To obtain the statistical error σ_K, we calculated the time autocorrelation function of monomer-monomer contacts, which displays a single-exponential decay with $\tau \approx 4$ μs. We then applied a block averaging procedure, using 7 independent blocks of length 2τ, to calculate the standard error in *K*. The error in the dimerization free energy $\Delta G = -RT \ln K$ is then obtained using $\sigma_{\Delta G} = RT / K \, \sigma_K$.

The dimerization free energy of -12 ± 2 kJ/mol we obtained for WALP23 in Ld can be compared to MARTINI simulations of W. L. Ash and coworkers (10). From potential of mean force calculations of WALP23 dimers in DOPC, a dimerization free energy of -15 kJ/mol was obtained, in good agreement with our value. In addition, both values also agree with the value of $\Delta G = -12.7 \pm 0.4$ kJ/mol obtained from FRET experiments of very similar peptides in DOPC (9). The peptides used in the experiments were X-(AALALAA)$_3$-Y, with X = 7-nitro-2-1, 3-benzoxadiazol-4-yl (NBD) and Y = NH_2 (I), or X = Ac and Y = $NHCH_2CH_2$-S-*N*-[4-[[4-(dimethylamino)phenyl]azo]-phenyl]maleimide (DABMI) (II), and FRET from I to II was measured.

References

1. Ramadurai S, *et al.* (2010) Influence of Hydrophobic Mismatch and Amino Acid Composition on the Lateral Diffusion of Transmembrane Peptides. *Biophys. J.* 99(5):1447-1454.
2. Ramadurai S, *et al.* (2009) Lateral diffusion of membrane proteins. *J Am Chem Soc* 131(35):12650-12656.
3. Risselada HJ & Marrink SJ (2008) The molecular face of lipid rafts in model membranes. *Proc. Natl. Acad. Sci. USA* 105(45):17367-17372.
4. Wong-Ekkabut J, *et al.* (2008) Computer Simulation study of fullerene translocation through lipid membranes. *Nature Nanotechnology* 3:363-368.
5. Hess B (2002) Determining the shear viscosity of model liquids from molecular dynamics simulations. *J. Chem. Phys.* 116(1):209-217.

6. Hess B & van der Vegt NFA (2006) Hydration thermodynamic properties of amino acid analogues: a systematic comparison of biomolecular force fields and water models. *J. Phys. Chem. B* 110(35):17616-17626.
7. Baron R, de Vries AH, Hünenberger PH, & van Gunsteren WF (2006) Configurational entropies of lipids in pure and mixed bilayers from atomic-level and coarse grained molecular dynamics simulations. *J. Phys. Chem. B* 110:15602-15614.
8. Baron R*, et al.* (2007) Comparison of thermodynamic properties of coarse-grained and atomic-level simulation models. *Chem. Phys. Chem.* 8:452-461
9. Yano Y & Matsuzaki K (2006) Measurement of Thermodynamic Parameters for Hydrophobic Mismatch 1: Self-Association of a Transmembrane Helix. *Biochemistry* 45(10):3370-3378.
10. Ash WL (2009) Helix-helix interactions in membrane proteins probed with computer simulations. PhD Thesis (University of Calgary, Canada).
11. MacKenzie KR, Prestegard JH, & Engelman DM (1997) A transmembrane helix dimer: structure and implications. *Science* 276(5309):131-133.
12. Holt A*, et al.* (2010) Order parameters of a transmembrane helix in a fluid bilayer: case study of a WALP peptide. *Biophys. J.* 98:1864-1872.
13. Esteban-Martin S & Salgado J (2007) The Dynamic Orientation of Membrane-Bound Peptides: Bridging Simulations and Experiments. *Biophys. J.* 93(12):4278-4288.
14. Sparr E*, et al.* (2005) Self-association of transmembrane alpha-helices in model membranes: importance of helix orientation and role of hydrophobic mismatch. *J. Biol. Chem.* 280(47):39324-39331.
15. Oostenbrink C, Villa A, Mark AE, & van Gunsteren WF (2004) A biomolecular force field based on the free enthalpy of hydration and solvation: The GROMOS force-field parameter sets 53A5 and 53A6. *J. Comput. Chem.* 25:1656-1676.
16. Xue Y (2010) The Effect of Environment on Peptide and Protein Folding: A Molecular Dynamics Study. PhD Thesis (University of Groningen, The Netherlands).
17. Marrink SJ, de Vries AH, Harroun TA, Katsaras J, & Wassall SR (2008) Cholesterol shows preference for the interior of polyunsaturated lipid membranes. *J. Am. Chem. Soc.* 130(1):10-11.
18. Berendsen HJC, Postma JPM, van Gunsteren WF, & Hermans J (1981) *Intermolecular Forces* (Reidel Publishing Company, Dordrecht, the Netherlands).
19. Rzepiela AJ*, et al.* (2010) Reconstruction of atomistic details from coarse-grained structures. *J. Comput. Chem.* 31(6):1333-1343.
20. Hess B (2008) P-LINCS: A parallel linear constraint solver for molecular simulation. *J. Chem. Theory Comput.* 4:116-122.
21. Hess B, Dekker H, Berendsen HJC, & Fraaie JGEM (1997) LINCS: A linear constraint solver for molecular simulations. *J. Comput. Chem.* 18:1463-1472.
22. Miyamoto S & Kollman PA (1992) SETTLE: An analytical version of the SHAKE and RATTLE algorithms for rigid water models. *J. Comput. Chem.* 13:952-962.
23. Tironi IG, Sperb R, Smith PE, & van Gunsteren WF (1995) A generalized reaction field method for molecular dynamics simulations. *J. Chem. Phys.* 102(13):5451-5459.
24. Knecht V & Grubmüller H (2003) Mechanical coupling via the membrane fusion SNARE protein syntaxin 1A: a molecular dynamics study. *Biophys. J.* 84:1527-1547.
25. Zhang W, Sloan-Lancaster J, Kitchen J, Trible RP, & Samelson LE (1998) LAT: the ZAP-70 tyrosine kinase substrate that links T cell receptor to cellular activation. *Cell* 92:83-92.
26. Zhang R, Trible RP, & Samelson LE (1998) LAT palmitoylation: its essential role in membrane microdomain targeting and tyrosine phosphorylation during T cell activation. *Immunity* 9:239-246.
27. Shogomori H*, et al.* (2005) Palmitoylation and intracellular domain interactions both contribute to raft targeting of linker for activation of T cells. *J. Biol. Chem.* 280(19):18931-18942.
28. van Duyl BY, Rijkers DTS, de Kruijff B, & Killian JA (2002) Influence of hydrophobic mismatch and palmitoylation on the association of transmembrane alpha-helical peptides with detergent-resistant membranes. *FEBS Lett.* 523(1-3):79-84.